Geochemistry Geophysics Geosystems G3
AN ELECTRONIC JOURNAL OF THE EARTH SCIENCES
Published by AGU and the Geochemical Society

Data Brief
Volume 4, Number 7
12 July 2003
8611, doi:10.1029/2002GC000469
ISSN: 1525-2027

Peridotites and gabbros from the Parece Vela backarc basin: Unique tectonic window in an extinct backarc spreading ridge

Yasuhiko Ohara
Hydrographic and Oceanographic Department of Japan, Tokyo 104-0045, Japan (ohara@jodc.go.jp)

Kantaro Fujioka
Japan Marine Science and Technology Center, Yokosuka 237-0061, Japan

Teruaki Ishii
Ocean Research Institute, University of Tokyo, Tokyo 164-8639, Japan

Hisayoshi Yurimoto
Department of Earth Sciences, Tokyo Institute of Technology, Tokyo 152-8551, Japan

[1] Peridotite samples from a backarc basin setting will help better understand global mid-oceanic ridge processes. Here we report detailed petrological data of serpentinized peridotite and gabbro from the extinct Parece Vela Basin in the Philippine Sea. Despite its relatively fast spreading rate (8.8–7.0 cm/y full-rate), the Parece Vela Basin spreading ridge (the Parece Vela Rift) has the distinct morpho-tectonic characteristics that indicate a small degree of mantle melting, including the presence of a huge mullion structure (the Godzilla Mullion). Peridotites in the Parece Vela Rift are exposed on the Godzilla Mullion as well as at a segment midpoint. The most notable characteristic of Parece Vela Rift peridotites is small-scale juxtaposition (i.e., a single-dredge-haul scale) of fertile peridotite and depleted peridotite (dunite and plagioclase-bearing peridotite). We interpret that the fertile peridotite (F-type) is the residue of a small degree of mantle melting (~4% near-fractional melting of a MORB-type mantle), whereas dunite (D-type) and plagioclase-bearing peridotite (P-type) are products of melt-mantle interaction. The associated evolved gabbros may represent the shallow level fractionated melt intruded into P-type. The distinct morpho-tectonic characteristics, peridotite exposure at a segment midpoint, and the presence of fertile peridotite may result from an extreme transform fault effect caused by the ridge-transform geometry of short first-order segments sandwiched by closely spaced fracture zones (“transform sandwich effect”).

Components: 9716 words, 8 figures, 10 tables.

Keywords: Backarc basin; peridotite; amagmatic tectonics; lithospheric process; megamullion.

Index Terms: 3640 Mineralogy and Petrology: Igneous petrology; 3035 Marine Geology and Geophysics: Midocean ridge processes; 1025 Geochemistry: Composition of the mantle.

Received 1 November 2002; **Revised** 6 May 2003; **Accepted** 13 May 2003; **Published** 12 July 2003.

Ohara, Y., K. Fujioka, T. Ishii, and H. Yurimoto, Peridotites and gabbros from the Parece Vela backarc basin: Unique tectonic window in an extinct backarc spreading ridge, *Geochem. Geophys. Geosyst.*, *4*(7), 8611, doi:10.1029/2002GC000469, 2003.

Theme: The Oman Ophiolite and Mid-Ocean Ridge Process
Guest Editors: Peter Kelemen, Chris MacLeod, and Susumu Umino

1. Introduction

[2] The study of backarc spreading systems has a strong bearing on two important aspects of the Earth's evolution, as it relates to both subduction zone and mid-oceanic ridge dynamics. However, this important tectonic setting is much less well understood than are arcs or mid-oceanic ridges.

[3] Serpentinized peridotites are important components of oceanic lithosphere and are exposed mostly at slow-spreading mid-oceanic ridges; these are referred to as abyssal peridotites [*Miyashiro et al.*, 1969; *Aumento and Loubat*, 1970; *Dick and Bullen*, 1984; *Dick et al.*, 1984; *Dick*, 1989]. Abyssal peridotites crop out at "tectonic windows" developed as major faults or escarpments on the seafloor. Observations at these tectonic windows provide important constraints on the architecture of oceanic lithosphere [*Cannat*, 1993; *Cannat et al.*, 1995], on the nature of the seafloor spreading process in time and space [*Tucholke and Lin*, 1994], and on the composition of oceanic lithosphere itself [*Dick et al.*, 1984; *Michael and Bonatti*, 1984].

[4] Abyssal peridotite is rarely reported from backarc basins (from the West Philippine Basin [*Shcheka et al.*, 1995], the Parece Vela Basin (PVB) [*Bogdanov*, 1977; *Dietrich et al.*, 1978; *Shcheka et al.*, 1995; *Ohara et al.*, 1996], and the Mariana Trough [*Bloomer et al.*, 1995; *Stern et al.*, 1996, 1997; *Ohara et al.*, 2002]; all basins are in the Philippine Sea), and the lack of samples has hindered our understanding of this important aspect of lithospheric evolution. We thus know relatively little directly about the deeper lithospheric architecture and composition of backarc basins.

[5] *Ohara et al.* [1996] reported the preliminary petrology of serpentinized peridotite and gabbro from the PVB. *Ohara et al.* [2001] then reported distinct bathymetric characteristics in the PVB spreading ridge (the Parece Vela Rift (PVR)), suggesting amagmatic extension was important in this relatively fast-spread backarc basin. Following these earlier studies, here we report detailed petrological data of serpentinized peridotite and gabbro from the PVR for the first time, and use the results to briefly discuss the lithospheric composition and processes beneath the PVR. Peridotite samples from various range of the spreading rate spectrum and spreading environment will help better understand global mid-oceanic ridge processes. In this regard, our data from a relatively fast-spread backarc basin are critical in a global context.

2. Geological Background

[6] The Philippine Sea occupies a large part of the western Pacific, which is composed of three large backarc basins separated by the Kyushu-Palau and the West Mariana ridges (both are remnant arcs; Figure 1). East of the Kyushu-Palau Ridge, the Shikoku Basin and the PVB are extinct backarc basins.

[7] The spreading history of the PVB consisted of two stages (Figure 2 [*Kasuga and Ohara*, 1997; *Okino et al.*, 1998, 1999], the first of which was E-W rifting and spreading with spreading axes trending N-S at ~26 Ma (spreading rate: 8.8 cm/y full-rate [*Okino et al.*, 1998, 1999]). The second stage involved counter-clockwise rotation of spreading axes from N-S to NW-SE at ~19 Ma (spreading rate: 7.0 cm/y full-rate (Y. Ohara, K. Okino, and T. Yoshida, Transform sandwich effect on mantle melting in oceanic spreading ridges: Transform fault effect in extremity, manuscript submitted to *Earth and Planetary Science Letters*, 2003, hereinafter referred to as Ohara et al., submitted manuscript, 2003)). Short length first-order segments (labeled as S1–S7 from south to north [*Ohara et al.*, 2001]) thus aligned en-echelon with closely spaced fracture zones. The spreading ceased at ~12 Ma (Ohara et al., submitted manuscript, 2003). The PVB opened relatively fast with "high" intermediate full-spreading rate 8.8–7.0 cm/y [*Ohara et al.*, 2001, submitted manuscript, 2003].

[8] The morpho-tectonic details of the basin were already reported elsewhere [*Kasuga and Ohara*, 1997; *Okino et al.*, 1998, 1999; *Ohara et al.*, 2001]. Although high magmatic budget is generally expected for a relatively fast-spreading ridge,

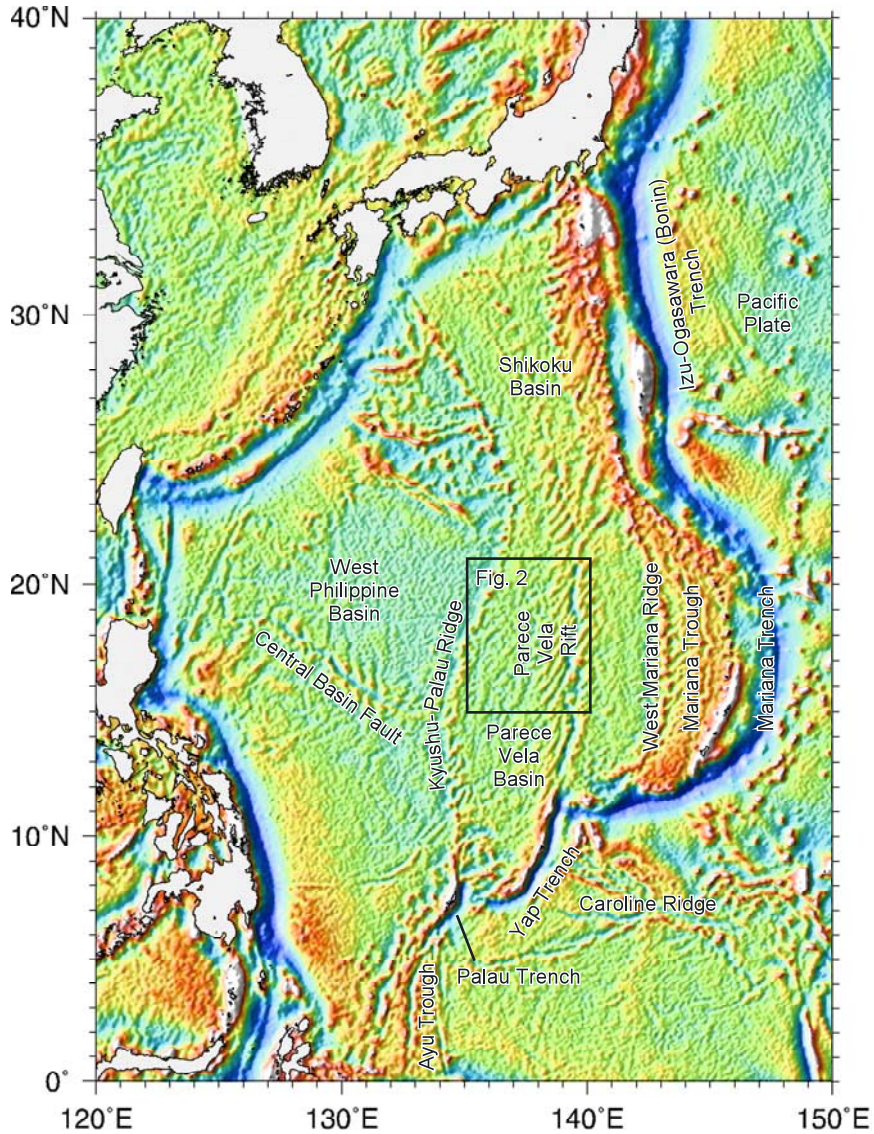

Figure 1. Satellite-derived free-air gravity filed showing the tectonic feature of Philippine Sea (data from [*Sandwell and Smith*, 1997]). Rectangle indicates the location of Figure 2.

Ohara et al. [2001] described the distinct morphotectonic characteristics of the PVR that indicate a small degree of mantle melting, despite the basin's relatively fast-spreading rate (Figure 2):

[9] 1. The axial rift valleys (nodal deeps) of the PVR have large water depth (maximum depth ~7500 m, which corresponds to ~6200 m zero-age depth after correction of 12 Ma subsidence [*Park et al.*, 1990]).

[10] 2. Megamullions develop at each segment (at least segments S1–S3). Recently discovered "megamullions" at slow-spreading ridges have been interpreted as exhumed footwalls of oceanic detachment faults in magma-starved ridge environments [*Cann et al.*, 1997; *Blackman et al.*, 1998; *Mitchell et al.*, 1998; *Tucholke et al.*, 1998; *MacLeod et al.*, 2002].

[11] 3. A huge megamullion named the Giant Megamullion ([*Ohara et al.*, 2003] renamed it the Godzilla Mullion) is observed at ~16°N; this is the largest known megamullion (~10 times larger in area than the Mid-Atlantic Ridge (MAR) megamullions).

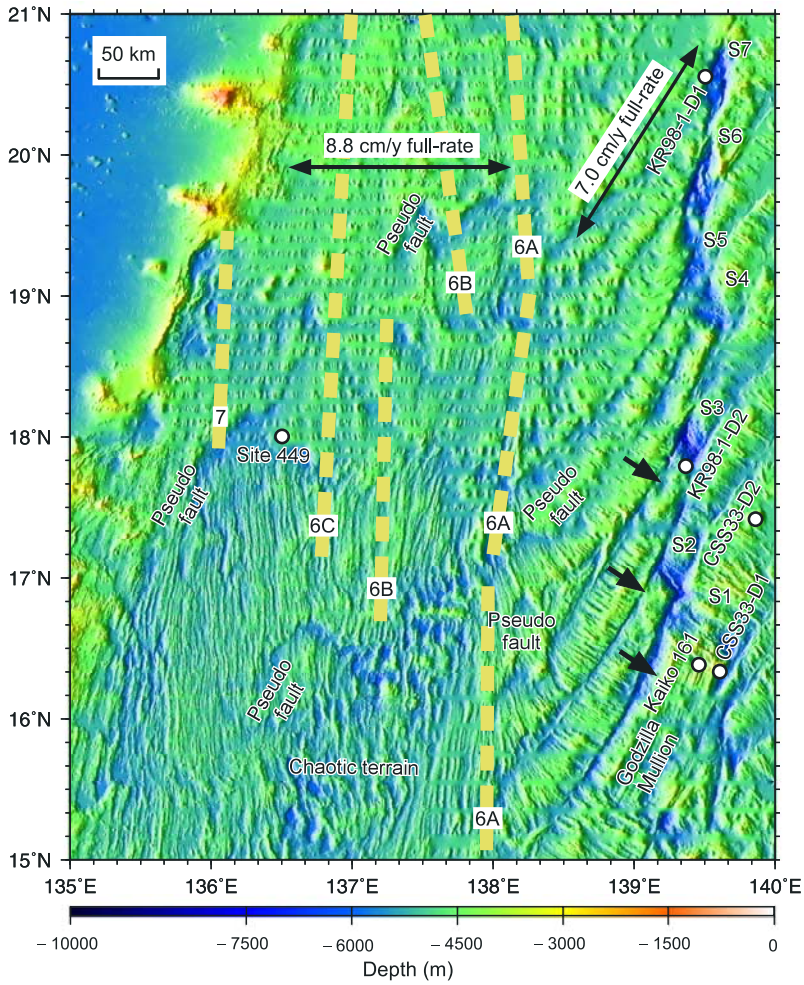

Figure 2. Interpreted shaded structural image of the Parece Vela Basin based on *Ohara et al.* [2001]. Dotted yellow lines are the magnetic anomaly isochrons with anomaly number taken from *Okino et al.* [1998, 1999]. The anomaly 7 corresponds to 26 Ma, and the anomaly 6A corresponds to 21 Ma [*Okino et al.*, 1998]. The full-spreading rates for the first stage of the basin evolution was 8.8 cm/y [*Okino et al.*, 1998], and for the second stage was 7.0 cm/y (Ohara et al., submitted manuscript, 2003). Some notable pseudofaults suggest high magmatic budget, consistent with the relatively fast-spreading rate [*Ohara et al.*, 2001]. The short, first-order segments (the right-stepping en-echelon diamond-shaped depressions in the central Parece Vela Basin; i.e., the Parece Vela Rift) are labeled as S1–S7 from south to north [*Ohara et al.*, 2001]. Distinct megamullions are indicated by short arrows, which develop along the full length of each segment (S1–S3) [*Ohara et al.*, 2001]. The Godzilla Mullion is characterized by the prominent axis-normal corrugations [*Ohara et al.*, 2001, 2003]. The chaotic terrain characterized by rough bathymetry is identified in the western Parece Vela Basin, also suggesting amagmatic extension occurred there [*Ohara et al.*, 2001]. Five sampling sites conducted by the authors along with Site 449 (during DSDP Leg 59) are shown. The two dredge hauls that recovered peridotites (CSS33-D1 and KR98-1-D2) are only considered in this paper. Note that dredge KR98-1-D2 was on the S3 segment midpoint.

[12] 4. These megamullions develop along the full length of each segment.

3. Samples

[13] Serpentinized peridotites and gabbros were dredged from the PVR for the first time in backarc basins by Russian scientists in 1976 [*Bogdanov*, 1977; *Dietrich et al.*, 1978] and in 1984 [*Shcheka et al.*, 1995]. However, no detailed petrological studies on these peridotite and gabbro samples have been published. Four dredge hauls and a single ROV dive were performed in the PVR by the authors (Table 1; Figure 2). Among these,

Table 1. List of the Sampling Sites in the Parece Vela Basin

Cruise	Sampling Method	Start			End			Setting	Lithologies Recovered	Total Weight, kg
		Latitude	Longitude	Depth, m	Latitude	Longitude	Depth, m			
S/V Takuyo (in 1995)	Dredge									
CSS33	D1	16°23.1′N	139°35.8′E	2659	16°23.3′N	139°35.1′E	2625	Godzilla Mullion	Peridotite, Gabbro	~4
CSS33	D2	17°24.5′N	139°51.1′E	3309	17°24.5′N	139°51.3′E	No record	Off axis seamount (Segment S1)	Mn-nodule	No record
R/V Kairei (in 1998)	Dredge									
KR98-1	D1	20°37.0′N	139°32.5′E	5500	20°37.4′N	139°32.2′E	5060	RTI (Segment S7)	Gabbro (two small pieces), Mn-nodule, Scoria	~1
KR98-1	D2	17°48.2′N	139°23.1′E	5852	17°47.9′N	139°22.4′E	5221	Segment midpoint (Segment S3)	Peridotite, Serpentine sandstone	~100
R/V Kairei (in 2000)	ROV Kaikodive									
KR00-3	161	16°25.0′N	139°27.5′E	5200	16°25.3′N	139°27.7′E	4938	Godzilla Mullion (Hanging wall)	Heavily altered basalt	~5

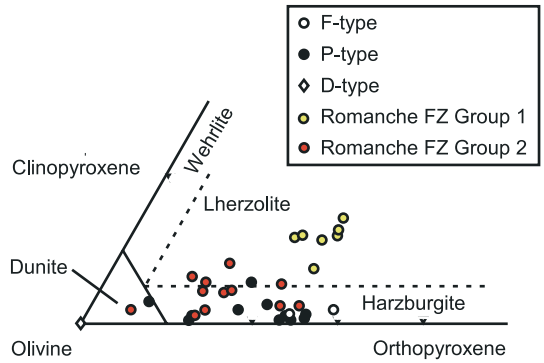

Figure 3. Modal composition of the Parece Vela Rift peridotites. Peridotites from the Romanche FZ are shown for comparison [*Seyler and Bonatti*, 1997]. Romanche FZ Group 1 peridotite is the fertile end-member whereas Group 2 is essentially plagioclase-bearing peridotite [*Seyler and Bonatti*, 1997].

dredge CSS33-D1 (by S/V Takuyo) at the northeastern end of the Godzilla Mullion recovered serpentinized peridotites and gabbros [*Ohara et al.*, 1996], whereas dredge KR98-1-D2 (by R/V Kairei) at the southwestern wall of the S3 segment midpoint a large amount of serpentinized peridotites (no gabbros were recovered).

[14] In this study, we utilized the peridotite and gabbro samples (total 38) from these two dredges. The samples from dredge CSS33-D1 are denoted as "33-001" etc., and from KR98-1-D2 are "D2-001" etc. (Table 2). On the basis of micro-topographic considerations on each dredge site, we infer that the lithologies recovered in CSS33-D1 are possibly from in situ outcrop, whereas those recovered in KR98-1-D2 are most likely from talus. In any case, the dredged samples give no information on the spatial relationships between different lithologies, and represent very small portions of lithosphere. Although the sample suite give only limited information, we may nevertheless use these mafic-ultramafic suites as a rare opportunity for understanding backarc basin lithospheric composition.

4. Petrography

4.1. Peridotites

[15] The degree of serpentinization of the studied peridotites are extensive, however it is often possible to estimate primary modal compositions

Table 2. List of the Studied Samples From the Parece Vela Rift

Dredge	Sample	Lithology	Interstitial Pl	Modal analysis	Type
Dredge CSS33-D1(Godzilla Mullion)	33-001	Harzburgite	Exist	Done	P
	33-002	Harzburgite	Exist	–	P
	33-003	Harzburgite	Exist	Done	P
	33-004	Harzburgite	Exist	Done	P
	33-005	Harzburgite	Exist	–	P
	33-006	Harzburgite	–	Done	P
	33-007	Harzburgite	–	Done	P
	33-008	Harzburgite	Exist	Done	P
	33-009	Harzburgite	Exist	Done	P
	33-010	Harzburgite	–	–	P
	33-011	Peridotite/Gabbro	–	–	–
	33-012	Harzburgite	Exist	Done	P
	33-013	Harzburgite	Exist	Done	P
	33-101	Gabbro	–	–	–
	33-201	Gabbro	–	–	–
	33-203	Gabbro	–	–	–
	33-207	Gabbro	–	–	–
	33-211	Gabbro	–	–	–
Dredge KR98-1-D2 (S3 segment midpoint)	D2-001	Dunite	–	Done	D
	D2-002	Dunite	–	–	D
	D2-003	Dunite	–	–	D
	D2-004	Dunite	–	–	D
	D2-005	Dunitic harzburgite	Exist	Done	P
	D2-010	Dunite	–	–	D
	D2-011	Dunite	–	–	D
	D2-014	Dunite	–	–	D
	D2-017	Harzburgite	–	Done	F
	D2-018	Harzburgite	–	Done	F
	D2-019	Dunite	–	Done	D
	D2-020	Dunite	–	Done	D
	D2-021	Dunite	–	Done	D
	D2-022	Dunite	–	–	D
	D2-023	Dunite	–	–	D
	D2-024	Dunite	–	–	D
	D2-025	Harzburgite	Exist	–	P
	D2-026	Dunite	–	Done	D
	D2-028	Lherzolite	Exist	Done	P
	D2-101	Harzburgite	–	–	P
	D2-102	Dunite	–	–	D
	D2-103	Harzburgite	Exist	–	P

P1, plagioclase.

by point counting. Primary modes of the peridotites along with the mean values from Vulcan and Bouvet fracture zones (FZ) peridotites (the American-Antarctic and Southwest Indian ridges, respectively; *Dick* [1989]), and Romanche FZ peridotites (the equatorial MAR; "Group 1" peridotites of *Seyler and Bonatti* [1997]) are listed in Table 3.

[16] On the basis of modal and mineral compositions, PVR peridotites are divided into three types (Tables 2 and 3; Figure 3). *F* (*Fertile*)-type (two samples: D2-017 and D2-018) peridotite is harzburgite with fertile mineral composition. P (*Plagioclase*)-type is generally plagioclase-bearing harzburgite and plagioclase-bearing dunitic harzburgite, which shows petrological evidence of melt-mantle interaction. Some peridotites not bearing plagioclase, but showing evidence of melt-mantle interaction are also assigned to P-type. P-type makes up all of the peridotite suite from dredge CSS33-D1. D-type is dunite, which makes up ~70% (by number) of the dredge KR98-1-D2 suite. To summarize, dredge CSS33-D1 recovered P-type peridotite (with gabbro), whereas dredge KR98-1-D2 recovered all three types of

Table 3. Representative Primary Modal Compositions of the Parece Vela Rift Peridotites

Vol%	Ol	Opx	Cpx	Sp	Pl	Total	Total points counted	Lithology	Type	Note
Dredge CSS33-D1 (Godzilla Mullion)										
33-001	75.2	22.9	0.2	0.3	1.4	100.0	3117	Harzburgite	P	Includes Phlog.
33-003	85.8	12.4	0.8	Tr.	1.0	100.0	3910	Harzburgite	P	
33-004	85.5	12.3	0.1	1.0	1.1	100.0	1348	Harzburgite	P	
33-006	80.3	17.6	1.6	0.3	0.2	100.0	1032	Harzburgite	P	
33-007	75.0	24.6	0.2	0.2	0.0	100.0	1289	Harzburgite	P	
33-008	76.3	20.5	2.2	1.0	0.0	100.0	1139	Harzburgite	P	
33-009	72.8	25.4	0.4	0.4	1.0	100.0	1969	Harzburgite	P	
33-012	70.4	25.2	1.0	1.6	1.8	100.0	797	Harzburgite	P	Includes Phlog. and Amp.
33-013	74.7	23.4	1.0	0.3	0.6	100.0	783	Harzburgite	P	
Dredge KR98-1-D2 (S3 segment midpoint)										
D2-017	69.3	28.8	1.5	0.4	0.0	100.0	2228	Harzburgite	F	Includes Amp.
D2-018	74.3	24.1	0.8	0.8	0.0	100.0	2559	Harzburgite	F	
D2-005	88.3	6.6	2.6	0.4	2.1	100.0	2884	Dunitic harzburgite	P	
D2-028	75.6	17.2	5.0	0.2	1.9	100.0	1644	Lherzolite	P	
D2-001	99.0	0.0	0.0	1.0	0.0	100.0	1310	Dunite	D	
D2-019	99.1	0.0	0.0	0.9	0.0	100.0	1514	Dunite	D	
D2-020	99.0	0.0	0.0	1.0	0.0	100.0	1523	Dunite	D	
D2-021	99.4	0.0	0.0	0.6	0.0	100.0	1586	Dunite	D	
D2-026	98.9	0.0	0.0	1.1	0.0	100.0	1800	Dunite	D	
Vulcan FZ mean	71.1	20.6	7.3	1.0	0.0	100.0	–	Lherzolite		
1 sigma	3.8	2.6	2.4	0.4	0.0	0.0	–			
Bouvet FZ mean	81.6	16.1	1.6	0.5	0.2	99.8	–	Harzburgite		
1 sigma	4.2	3.4	1.3	0.3	0.4	4.8	–			
Romanche FZ mean	65.0	22.3	11.2	1.6	0.0	100.0	–	Lherzolite		
1 sigma	3.1	2.3	2.3	0.7	0.0	0.0	–			

Ol, olivine; Opx, orthopyroxene; Cpx, clinopyroxene; Sp, spinel; Pl, plagioclase; Phlog, phlogopite; Amp, amphibole. Each analysis is performed on 0.67 mm × 0.60 mm grid interval; no correction for differential volume expansion during serpentinization has been made. Mean Vulcan and Bouvet FZ data are from *Dick* [1989]; mean Romanche FZ data are from "Group 1" peridotites of *Seyler and Bonatti* [1997].

peridotites mixed together (without gabbro) (Tables 1 and 2).

[17] The primary relict minerals are orthopyroxene, clinopyroxene and spinel (Figures 4a and 4b); relict olivine is not preserved for all three types of peridotites. The primary mineral assemblages are slightly deformed and the freshest portions of the rocks exhibit porphyloclastic textures. Spinels in F-type are yellowish-brown (Figure 4a), and have the least-depleted chemical compositions among the PVR peridotite suites. P-type includes irregular dark-brown patches of hydrogrossular with high Ca and Al contents [*Ohara et al.*, 1996], that appear to be altered plagioclase (Figure 4c). Plagioclase-bearing peridotites are well described in the Romanche FZ (Figure 4d [*Dick*, 1989; *Bonatti et al.*, 1992, 1993; *Seyler and Bonatti*, 1997]). Interstitial amphibole is present in some F- and P-types (Figure 4e). Phlogopite occurs as patches in orthopyroxene in two P-type samples (Figure 4f). D-type consists of totally serpentinized olivine and spinel.

4.2. Gabbros

[18] Nearly half of the samples recovered from dredge CSS33-D1 are gabbros. No gabbros were recovered from dredge KR98-1-D2 (Tables 1 and 2).

[19] Parece Vela Rift gabbros are relatively fresh and evolved, and contain clinopyroxene and plagioclase as primary relict minerals. Some gabbros contain olivines, most of which are altered to talc and tremolite. Some plagioclase grains have kink-bands, and are partly recrystallized in polygonal grains (Figure 4g). Parece Vela Rift gabbros also contain abundant red-brown amphibole, occurring both as primary phases and as rims on clinopyroxene (Figure 4h).

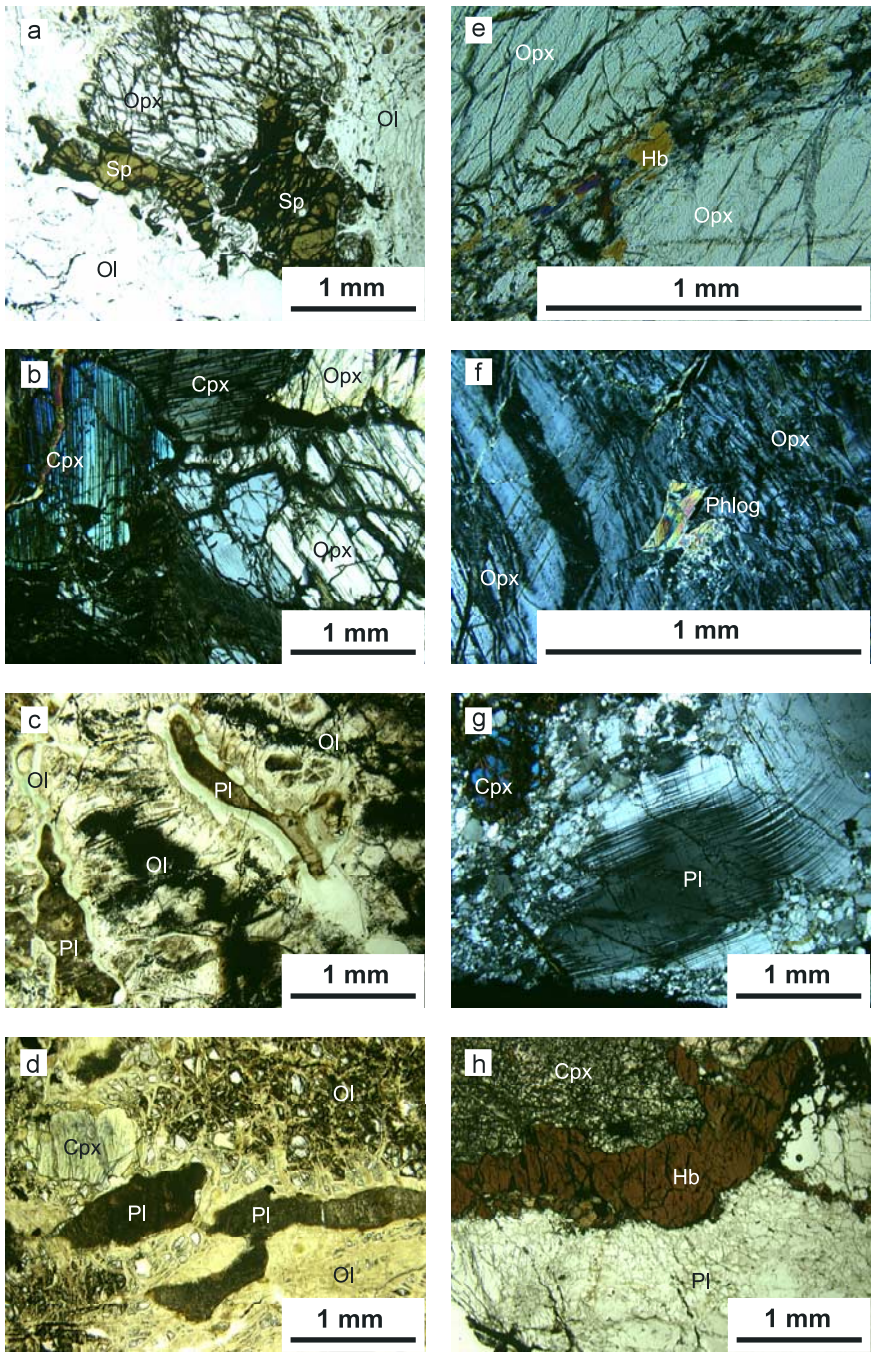

Figure 4. Microphotographs of thin sections all taken with transmitted light. (a) Common habit of orthopyroxene and spinel in F-type. Sample D2-018, plane-polarized light. Note the yellowish-brown spinel. (b) Common habit of orthopyroxene and clinopyroxene in peridotite. Sample D2-028 (P-type), crossed polarizers. (c) Altered plagioclase in P-type. Sample 33-001, plane-polarized light. Note that no relict olivine remains. (d) Altered plagioclase in Romanche FZ peridotite. Sample AII-20-17-30 (from the Woods Hole Oceanographic Institution; *Dick and Bullen* [1984]; courtesy of H. Dick), plane-polarized light. (e) Pargasite vein in orthopyroxene in peridotite. Sample 33-012 (P-type), crossed polarizers. (f) Phlogopite patch in orthopyroxene in peridotite. Sample 33-012 (P-type), crossed polarizers. (g) Kinked and recrystallized plagioclase in gabbro. Sample 33-207, crossed polarizers. (h) Red-brown hornblende in gabbro. Sample 33-207, plane-polarized light. Ol, olivine; Opx, orthopyroxene; Cpx, clinopyroxene; Sp, spinel; Pl, plagioclase; Hb, hornblende; Phlog, phlogopite.

Table 4. Electron Probe Analyses of Spinel in the Parece Vela Rift Peridotites

	Godzilla Mullion, P-Type								S3 Segment Midpoint														
									F-Type		P-Type					D-Type							
Sample	33-001	33-004	33-006	33-007	33-008	33-009	33-012	33-013	D2-017	D2-018	D2-005	D2-025	D2-028	D2-101	D2-103	D2-001	D2-019	D2-020	D2-021	D2-023	D2-024	D2-026	D2-102
No. Anal.	6	58	40	45	76	50	101	7	30	9	24	22	19	27	25	81	12	16	6	12	38	30	14
											Given in wt%												
TiO_2	0.92	0.17	0.40	0.28	0.30	0.36	0.38	0.37	0.04	0.06	0.64	0.00	0.23	0.15	0.42	0.37	0.28	0.37	0.29	0.26	0.32	0.22	0.32
Al_2O_3	17.22	32.99	24.84	26.35	26.40	25.70	29.52	25.80	51.62	52.26	26.26	38.96	31.65	38.91	25.20	30.60	32.71	30.57	33.81	30.69	30.11	39.38	31.97
FeO	21.88	13.10	15.72	13.66	14.93	15.52	13.67	15.50	11.48	10.96	17.20	12.80	14.58	13.20	17.22	16.73	14.03	16.75	13.76	14.27	14.28	12.38	15.82
Fe_2O_3	4.40	1.90	2.51	1.48	1.72	2.61	2.33	3.08	2.01	1.43	3.96	1.55	2.17	1.23	4.29	4.53	2.77	3.69	3.68	3.56	6.17	3.24	2.98
MnO	0.32	0.21	0.18	0.18	0.12	0.17	0.19	0.22	0.12	0.15	0.18	0.12	0.17	0.15	0.19	0.20	0.16	0.21	0.17	0.13	0.15	0.15	0.18
MgO	9.32	15.87	13.60	15.05	14.37	13.81	15.54	14.03	18.64	18.97	13.07	16.51	14.98	16.61	12.65	13.53	15.46	13.36	15.70	15.07	14.59	16.84	14.09
CaO	0.01	0.00	0.00	0.00	0.00	0.01	0.00	0.00	0.00	0.00	0.01	0.01	0.00	0.00	0.00	0.00	0.00	0.00	0.00	0.00	0.03	0.01	0.01
Cr_2O_3	45.64	35.86	42.12	43.32	42.72	41.95	39.01	41.89	16.04	15.81	38.80	30.28	36.80	29.49	40.16	34.43	35.14	34.90	33.05	36.48	33.14	27.17	34.56
NiO	0.13	0.14	0.20	0.11	0.15	0.16	0.15	0.14	0.30	0.34	0.17	0.17	0.14	0.24	0.19	0.13	0.17	0.20	0.23	0.15	0.18	0.28	0.20
Total	99.84	100.25	99.57	100.42	100.70	100.30	100.79	101.04	100.24	99.99	100.28	100.41	100.71	99.98	100.32	100.52	100.73	100.06	100.69	100.62	98.98	99.66	100.13
Mg #	0.452	0.689	0.620	0.671	0.641	0.624	0.681	0.629	0.745	0.758	0.592	0.697	0.653	0.701	0.578	0.599	0.671	0.597	0.679	0.660	0.653	0.714	0.622
1 sigma (Mg #)	0.012	0.008	0.032	0.006	0.017	0.020	0.028	0.007	0.010	0.013	0.020	0.009	0.008	0.008	0.014	0.030	0.008	0.005	0.006	0.007	0.013	0.006	0.007
Cr #	0.640	0.422	0.532	0.524	0.521	0.523	0.470	0.521	0.172	0.169	0.498	0.343	0.438	0.337	0.517	0.432	0.419	0.434	0.396	0.444	0.425	0.316	0.420
1 sigma (Cr #)	0.007	0.011	0.007	0.008	0.013	0.010	0.011	0.003	0.006	0.007	0.014	0.010	0.006	0.015	0.005	0.032	0.005	0.005	0.004	0.008	0.007	0.003	0.005

No. Anal., Number of analyses making up the average composition.

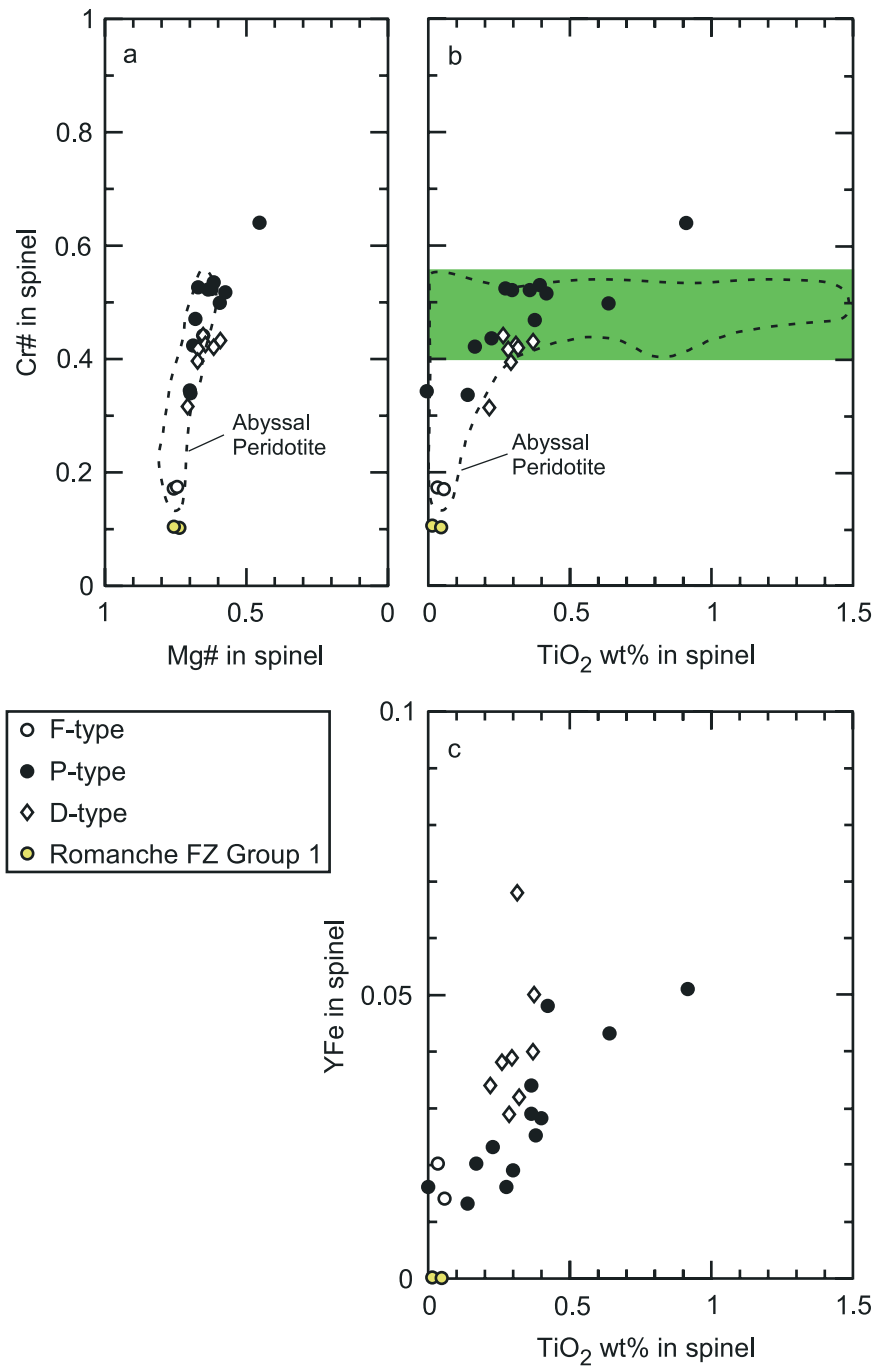

Figure 5. Spinel compositional plots for Parece Vela Rift peridotites, with fields for abyssal peridotite for comparison [*Dick and Bullen*, 1984]. Romanche FZ Group 1 peridotite [*Seyler and Bonatti*, 1997; the mineral data from *Bonatti et al.*, 1993] is also plotted for comparison. (a) Mg # versus Cr #. The Cr # of spinel in peridotites is a good indicator of the degree of melting [*Dick and Bullen*, 1984], with low Cr # spinels representing less-depleted peridotite and high Cr # spinels representing more-depleted peridotite. (b) TiO_2 wt% versus Cr # in spinel. Note that P- and D-types have higher TiO_2 content. Hatched area is the range for most abyssal plagioclase-bearing peridotites [*Dick and Bullen*, 1984]. Spinels in plagioclase-bearing peridotites are richer in Ti and Fe^{3+} and tend to be more Cr-rich compared to plagioclase-free peridotites from the same locality [*Dick and Bullen*, 1984; *Seyler and Bonatti*, 1997]. (c) TiO_2 wt% versus YFe (= $Fe^{3+}/(Fe^{3+} + Al + Cr)$) in spinel. Note that TiO_2 wt% and YFe correlate in P- and D-types.

Table 5. Electron Probe Analyses of Orthopyroxene in the Parece Vela Rift Peridotites and Gabbros

	Godzilla Mullion									S3 Segment Midpoint					
	P-Type								Gabbro	F-Type		P-Type			
Sample	33-001	33-004	33-005	33-007	33-008	33-009	33-012	33-013	33-011	D2-017	D2-018	D2-005	D2-028	D2-101	D2-103
No. Anal.	5	16	65	85	9	52	30	70	6	68	84	90	33	14	19
							Give in wt%								
SiO_2	54.61	54.85	55.60	54.80	54.48	54.33	54.76	56.13	55.21	54.04	54.56	55.10	53.98	55.53	54.11
TiO_2	0.13	0.03	0.10	0.11	0.08	0.08	0.12	0.11	0.10	0.09	0.08	0.17	0.09	0.08	0.11
Al_2O_3	5.00	4.00	3.18	3.60	4.11	3.99	3.99	2.71	2.61	5.04	4.93	2.54	3.06	4.18	3.29
FeO	5.70	5.42	5.71	5.25	5.39	6.03	5.62	5.65	9.48	5.75	5.94	6.42	6.06	5.38	6.61
MnO	0.11	0.17	0.14	0.18	0.08	0.10	0.17	0.14	0.23	0.11	0.16	0.13	0.10	0.13	0.15
MgO	32.57	33.04	32.88	33.15	33.09	33.16	32.07	32.71	30.84	32.79	32.68	32.80	33.23	31.86	32.06
CaO	1.89	1.52	1.28	1.61	1.76	1.23	2.30	2.04	1.57	1.82	1.32	1.44	1.60	2.62	1.70
Na_2O	0.09	0.03	0.03	0.05	0.06	0.10	0.08	0.06	0.08	0.07	0.00	0.04	0.05	0.11	0.04
Cr_2O_3	1.04	0.97	1.06	1.00	1.02	1.01	1.04	0.92	0.92	0.66	0.66	0.73	0.83	0.92	0.89
NiO	0.08	0.14	0.07	0.07	0.13	0.11	0.13	0.07	0.08	0.08	0.12	0.13	0.11	0.10	0.08
Total	101.23	100.18	100.04	99.83	100.21	100.14	100.28	100.55	101.12	100.43	100.46	99.50	99.09	100.91	99.04
Mg #	0.911	0.916	0.911	0.918	0.916	0.907	0.911	0.912	0.853	0.910	0.908	0.901	0.907	0.914	0.896
1 sigma (Mg #)	0.003	0.002	0.004	0.003	0.003	0.004	0.002	0.002	0.004	0.002	0.003	0.003	0.002	0.003	0.002
En	87.7	88.9	88.9	89.0	88.5	88.6	87.0	87.6	82.7	87.9	88.4	87.6	88.0	86.6	86.7
Fs	8.6	8.2	8.7	7.9	8.1	9.0	8.5	8.5	14.3	8.6	9.0	9.6	9.0	8.2	10.0
Wo	3.7	2.9	2.5	3.1	3.4	2.4	4.5	3.9	3.0	3.5	2.6	2.8	3.0	5.1	3.3

No. Anal., Number of analyses making up the average composition. En, enstatite content; Fs, ferrosilite content; Wo, wollastonite content.

Table 6a. Electron Probe Analyses of Clinopyroxene in the Parece Vela Rift Peridotites

	Godzilla Mullion, P-Type								S3 Segment Midpoint					
									F-Type		P-Type			
Sample	33-001a	33-001b	33-005	33-006	33-008	33-009	33-012	33-013	D2-017	D2-018	D2-005	D2-028	D2-101	D2-103
No. Anal.	25	18	49	53	5	20	5	15	29	20	22	34	15	13
							Give in wt%							
SiO_2	51.04	51.93	51.92	50.91	51.20	52.16	51.50	52.28	50.61	51.06	51.55	50.28	52.42	51.37
TiO_2	0.35	1.44	0.30	0.25	0.22	0.23	0.36	0.28	0.27	0.26	0.39	0.21	0.24	0.40
Al_2O_3	6.19	2.92	4.75	3.53	6.25	2.95	5.18	3.83	6.38	6.07	4.08	5.21	5.37	3.71
FeO	2.56	5.04	2.46	2.56	2.89	2.65	2.59	2.53	2.61	2.71	3.14	3.13	2.54	3.37
MnO	0.05	0.16	0.09	0.07	0.05	0.11	0.08	0.13	0.05	0.13	0.08	0.06	0.08	0.09
MgO	16.01	16.12	16.56	18.97	17.16	16.48	15.81	16.93	16.29	16.36	16.98	17.30	16.18	16.00
CaO	22.61	21.32	22.19	20.06	21.23	22.48	22.45	21.70	22.07	22.28	21.22	21.41	21.87	21.52
Na_2O	0.56	0.82	0.40	0.43	0.50	0.86	0.59	0.63	0.61	0.32	0.53	0.37	0.75	0.73
Cr_2O_3	1.50	0.47	1.63	1.28	1.70	1.49	1.55	1.50	1.13	1.01	1.39	1.33	1.50	1.49
NiO	0.04	0.01	0.03	0.13	0.06	0.06	0.02	0.07	0.04	0.07	0.09	0.06	0.06	0.02
Total	100.91	100.24	100.33	98.19	101.24	99.46	100.12	99.85	100.05	100.26	99.44	99.37	101.02	98.72
Mg #	0.918	0.851	0.923	0.930	0.914	0.917	0.916	0.923	0.918	0.915	0.906	0.908	0.919	0.894
1 sigma (Mg #)	0.003	0.018	0.008	0.007	0.004	0.009	0.002	0.004	0.004	0.007	0.009	0.007	0.004	0.004
En	47.5	47.0	48.9	54.5	50.4	48.3	47.3	49.9	48.5	48.3	49.9	50.2	48.5	48.0
Fs	4.3	8.3	4.1	4.1	4.8	4.4	4.3	4.2	4.4	4.5	5.2	5.1	4.3	5.7
Wo	48.2	44.7	47.1	41.4	44.8	47.4	48.3	45.9	47.2	47.3	44.9	44.7	47.2	46.4

No. Anal., Number of analyses making up the average composition. En, enstatite content; Fs, ferrosilite content; Wo, wollastonite content. Clinopyroxene in 33-001 retains two different disequilibrium compositions (denoted as a and b).

Table 6b. Electron Probe Analyses of Clinopyroxene in the Parece Vela Rift Gabbros

	Godzilla Mullion													
Sample	33-011a	33-011b	33-101a	33-101b	33-201a	33-201b	33-201c	33-202a	33-202b	33-202c	33-203	33-207	33-211a	33-211b
No. Anal.	10	51	10	23	10	7	15	11	7	6	11	26	5	7
							Given in wt%							
SiO_2	54.13	53.44	52.65	52.32	52.87	51.76	51.90	53.09	52.31	51.14	50.62	51.57	53.20	50.76
TiO_2	0.29	0.31	0.66	0.83	0.74	1.31	1.23	0.69	1.09	1.24	0.90	1.18	0.07	1.23
Al_2O_3	2.02	2.94	3.14	3.13	2.58	3.14	3.04	2.21	3.17	3.87	3.15	2.72	0.46	3.06
FeO	3.86	4.39	5.73	6.68	7.13	7.87	8.30	7.09	7.63	8.16	7.08	9.37	7.56	9.23
MnO	0.17	0.19	0.18	0.23	0.22	0.23	0.26	0.23	0.24	0.24	0.16	0.33	0.32	0.28
MgO	16.59	16.10	15.97	16.11	15.94	14.93	14.19	14.88	14.84	14.67	15.55	13.68	14.39	13.68
CaO	21.74	21.16	20.79	20.11	20.47	20.76	20.91	21.75	20.56	19.32	20.94	20.75	23.14	20.36
Na_2O	0.68	0.79	0.52	0.52	0.48	0.52	0.60	0.71	0.91	1.17	0.58	0.48	0.26	0.71
Cr_2O_3	1.19	1.48	0.05	0.06	0.03	0.03	0.00	0.00	0.00	0.00	0.00	0.01	0.02	0.01
NiO	0.08	0.06	0.01	0.01	0.02	0.05	0.02	0.02	0.04	0.03	0.02	0.01	0.01	0.01
Total	100.76	100.85	99.69	100.01	100.48	100.61	100.45	100.67	100.78	99.84	99.00	100.10	99.42	99.34
Mg #	0.885	0.867	0.832	0.811	0.800	0.772	0.753	0.789	0.776	0.762	0.797	0.722	0.773	0.726
1 sigma (Mg #)	0.004	0.009	0.006	0.010	0.007	0.003	0.008	0.016	0.014	0.013	0.007	0.008	0.016	0.021
En	48.3	47.7	46.8	46.9	46.0	43.6	41.9	43.1	43.8	44.3	45.0	40.4	40.8	40.8
Fs	6.3	7.3	9.4	10.9	11.5	12.9	13.7	11.5	12.6	13.8	11.5	15.5	12.0	15.5
Wo	45.4	45.0	43.8	42.1	42.5	43.5	44.4	45.3	43.6	41.9	43.5	44.1	47.2	43.7

No. Anal., Number of analyses making up the average composition. En, enstatite content; Fs, ferrosilite content; Wo, wollastonite content. Clinopyroxene in 33-011, 33-101, 33-201, 33-202 and 33-211 retains several different disequilibrium compositions (denoted as a, b and c).

5. Mineral Chemistry

[20] Minerals were analyzed with a JEOL JCXA-733 electron microprobe at the Ocean Research Institute, the University of Tokyo. Analytical condition is described in *Ohara et al.* [2002] with correction procedure after *Bence and Albee* [1968]. The mineral compositions presented in this paper are averages of multiple core analyses.

5.1. Spinel

[21] The spinel data are listed in Table 4. A plot of Mg/(Mg + Fe) ratio (= Mg #) versus Cr/(Cr + Al) ratio (= Cr #) in spinel is shown in Figure 5a. F-type spinels with Cr # ~0.17 plot at the near least-depleted end of the abyssal peridotite compositional range defined by *Dick and Bullen* [1984]. On the other hand, P- and D-types spinels show more depleted composition. P-type spinel is generally more Cr- and Fe-rich than D-type. There are no samples having spinel of intermediate composition between F-type, and P- and D-types.

[22] TiO_2 content of spinel from F-type is almost negligible (Figure 5b), whereas that of P- and D-types are generally high (average ~0.35 wt%). TiO_2 content of spinel in P- and D-types also correlate with $Fe^{3+}/(Cr + Al + Fe^{3+})$ ratio (= YFe) (Figure 5c).

5.2. Pyroxenes

[23] The orthopyroxene and clinopyroxene data are listed in Tables 5 and 6A, 6B. Figures 6a–6c show Mg # versus Al_2O_3, Cr_2O_3 and TiO_2 in orthopyroxene, respectively. F-type orthopyroxenes generally plot in the fertile end of the main cluster defined by the Atlantic and Indian ocean peridotites. Figures 7a–7d show Mg # versus Al_2O_3, Cr_2O_3, TiO_2 and Na_2O in clinopyroxene, respectively. Again, F-type clinopyroxenes generally plot in the fertile end of the main cluster defined by the Atlantic and Indian ocean peridotites (excluding Na_2O). The gabbroic pyroxene data show the distinctly fractionated nature of PVR gabbros (Figures 6a–6c; 7a–7d).

5.3. Plagioclase

[24] The inferred plagioclase in P-type peridotite is totally altered and we cannot know the original composition. The gabbroic plagioclase data are

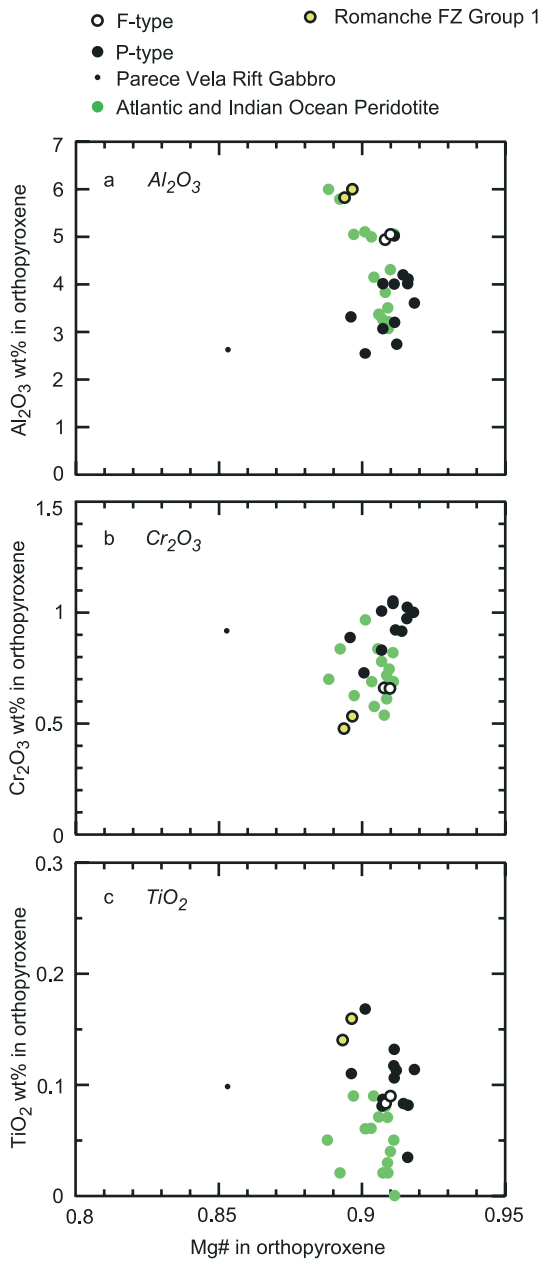

Figure 6. Orthopyroxene compositional plots for Parece Vela Rift peridotites and gabbro, with fields for Atlantic and Indian ocean peridotites for comparison (data from [*Bonatti et al.*, 1992; *Cannat et al.*, 1992; *Cannat and Seyler*, 1995; *Johnson et al.*, 1990; *Johnson and Dick*, 1992; *Ross and Elthon*, 1997]). Romanche FZ Group 1 peridotite [*Seyler and Bonatti*, 1997; the mineral data from *Bonatti et al.*, 1993] is also plotted for comparison. (a) Mg # versus Al_2O_3 wt%. (b) Mg # versus Cr_2O_3 wt%. (c) Mg # versus TiO_2 wt%.

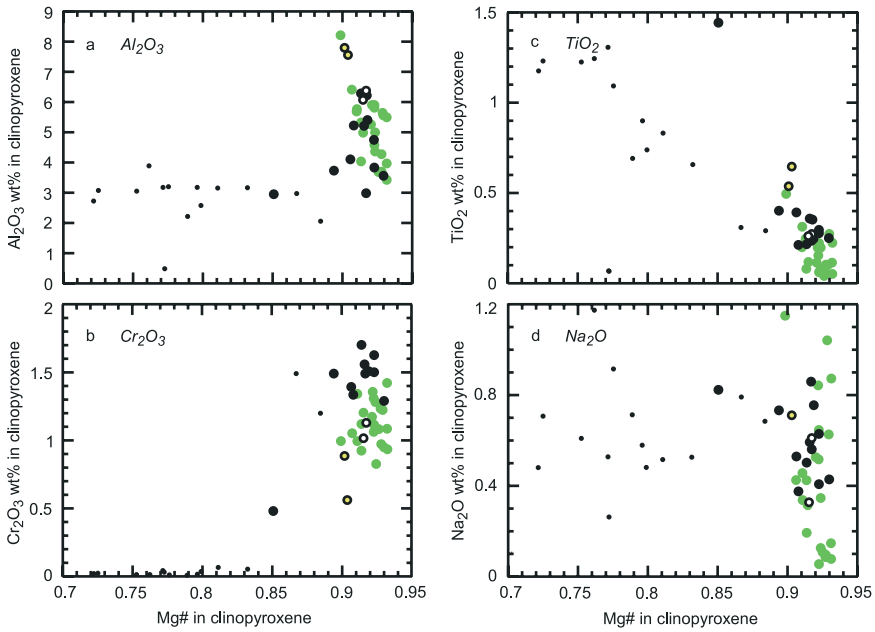

Figure 7. Clinopyroxene compositional plots for Parece Vela Rift peridotites and gabbro, with fields for Atlantic and Indian ocean peridotites for comparison (data from [*Bonatti et al.*, 1992; *Cannat et al.*, 1992; *Cannat and Seyler*, 1995; *Johnson et al.*, 1990; *Johnson and Dick*, 1992; *Ross and Elthon*, 1997]). Romanche FZ Group 1 peridotite [*Seyler and Bonatti*, 1997; the mineral data from *Bonatti et al.*, 1993] is also plotted for comparison. Symbols as in Figure 6. (a) Mg # versus Al_2O_3 wt%. (b) Mg # versus Cr_2O_3 wt%. (c) Mg # versus TiO_2 wt%. (d) Mg # versus Na_2O wt%.

Table 7. Electron Probe Analyses of Plagioclase in the Parece Vela Rift Gabbros

	Godzilla Mullion							
Sample	33-101	33-201	33-202	33-203a	33-203b	33-207	33-211a	33-211b
No. Anal.	40	24	12	5	10	8	8	5
				Given in wt%				
SiO_2	55.47	56.63	56.80	54.70	56.14	58.99	57.38	62.38
TiO_2	0.07	0.08	0.08	0.09	0.07	0.09	0.09	0.00
Al_2O_3	28.59	27.61	27.85	28.19	26.89	26.12	26.71	23.10
FeO	0.25	0.21	0.15	0.20	0.21	0.19	0.18	0.03
MnO	0.04	0.02	0.01	0.00	0.00	0.02	0.01	0.01
MgO	0.05	0.01	0.00	0.04	0.04	0.00	0.01	0.00
CaO	10.87	10.27	10.31	10.70	9.34	8.31	8.81	4.47
Na_2O	5.42	5.82	5.85	5.86	6.55	6.81	6.43	8.95
K_2O	0.07	0.14	0.17	0.11	0.15	0.20	0.21	0.07
Cr_2O_3	0.01	0.00	0.00	0.00	0.00	0.01	0.01	0.00
NiO	0.03	0.01	0.01	0.02	0.03	0.01	0.00	0.01
Total	100.87	100.80	101.25	99.90	99.41	100.76	99.83	99.01
An	52.3	49.0	48.9	50.0	43.7	39.8	42.6	21.6
Ab	47.2	50.2	50.1	49.5	55.4	59.0	56.2	78.0
Or	0.4	0.8	1.0	0.6	0.9	1.2	1.2	0.4
1 sigma (An)	2.0	2.0	0.7	0.9	0.8	1.1	3.3	7.7

No. Anal., Number of analyses making up the average composition. An, anorthite content; Ab, albite content; Or, orthoclase content.

Table 8. Electron Plobe Analyses of Amphibole in the Parece Vela Rift Peridotites

	Godzilla Mullion, P-Type								S3 Segment Midpoint, F-Type								Zabargad Island, Amphibole Peridotite		
Sample	33-001a	33-001b	33-001c	33-006a	33-006b	33-008	33-012a	33-012b	D2-017a	D2-017b	D2-017c	D2-017d	D2-017e	D2-017f	D2-017g	D2-017h	Z-35	Z-206a	Z-206b
No. Anal.	33	6	15	15	5	14	5	11	28	19	4	7	11	11	7	2	-	-	-
									Given in wt%										
SiO_2	45.31	48.71	45.01	57.57	54.87	56.61	52.39	44.05	54.13	54.69	53.65	52.37	50.48	46.93	44.70	45.73	43.70	48.60	48.40
TiO_2	0.54	2.26	4.19	0.04	0.04	0.02	0.46	3.92	0.10	0.09	0.15	0.24	0.24	0.33	0.58	0.50	3.53	0.06	0.05
Al_2O_3	12.10	7.32	9.64	0.35	1.82	1.20	5.94	11.19	2.82	2.34	4.30	4.40	6.23	11.12	13.52	11.54	12.70	8.34	8.21
FeO	3.48	4.62	6.78	2.04	2.32	2.16	2.67	3.42	2.40	2.46	2.79	3.12	3.22	3.52	3.82	4.30	4.82	4.51	4.32
MnO	0.03	0.07	0.11	0.07	0.05	0.04	0.20	0.44	0.05	0.07	0.03	0.17	0.03	0.03	0.03	0.06	0.09	0.07	0.04
MgO	18.94	19.20	16.70	24.27	23.62	24.63	21.42	17.59	23.62	23.69	22.58	22.31	21.75	19.68	18.53	19.15	16.90	20.90	21.00
CaO	11.55	12.20	11.78	12.60	12.53	12.80	12.51	11.74	12.35	12.70	12.87	12.08	12.72	11.99	12.49	12.34	12.40	9.90	10.30
Na_2O	3.04	2.09	2.82	0.18	0.58	0.25	1.30	2.90	0.77	0.64	1.07	1.20	1.49	2.24	2.97	2.71	2.86	2.19	2.21
K_2O	0.48	0.30	0.48	0.01	0.03	0.01	0.09	0.84	0.07	0.05	0.11	0.06	0.04	0.03	0.02	0.13	0.91	0.45	0.37
Cr_2O_3	2.44	0.88	0.39	0.02	0.00	0.02	0.58	2.01	0.53	0.41	0.69	1.00	0.93	1.05	0.86	1.30	0.40	2.00	1.65
NiO	0.09	0.07	0.05	0.21	0.26	0.18	0.17	0.17	0.05	0.05	0.07	0.04	0.08	0.09	0.12	0.10	0.07	0.12	0.13
Total	98.01	97.72	97.93	97.36	96.11	97.93	97.74	98.28	96.87	97.19	98.29	97.00	97.20	97.02	97.65	97.85	98.38	97.14	96.68
Mg #	0.906	0.879	0.814	0.955	0.948	0.953	0.933	0.902	0.946	0.945	0.935	0.927	0.923	0.909	0.896	0.888	0.862	0.892	0.897
1 sigma (Mg #)	0.006	0.030	0.019	0.004	0.007	0.001	0.020	0.000	0.004	0.007	0.013	0.011	0.012	0.007	0.008	0.008	-	-	-

No. Anal., Number of analyses making up the average composition. Amphibole in Parece Vela Rift peridotites (except in 33-008) retains several different disequilibrium compositions (denoted as a to h). Amphibole data from Zabargad Island amphibole peridotite are from *Bonatti et al.* [1986].

Table 9. Electron Probe Analyses of Phlogopite in the Parece Vela Rift Peridotites

	Godzilla Mullion, P-Type	
Sample	33-001	33-012
No. Anal.	13	13
	Given in wt%	
SiO_2	39.39	38.73
TiO_2	0.17	1.69
Al_2O_3	15.67	15.96
FeO	3.63	3.29
MnO	0.02	0.06
MgO	25.47	24.28
CaO	0.09	0.02
Na_2O	1.80	1.15
K_2O	6.12	7.54
Cr_2O_3	1.46	1.67
NiO	0.22	0.24
Total	94.05	94.63
Mg #	0.926	0.929
1 sigma (Mg #)	0.009	0.003
Cr #	0.059	0.066
1 sigma (Cr #)	0.006	0.003
K#	0.691	0.811
1 sigma (K #)	0.032	0.009

No. Anal., Number of analyses making up the average composition K # = K/(K + Na).

listed in Table 7. These plagioclases have fractionated anorthite contents (An = ~20–50).

5.4. Hydrous Minerals in Peridotites

[25] Amphibole is present in five samples both in F- and P-types (Table 8). The composition is quite variable in each sample, ranging from "primary (i.e., not related to "late stage" serpentinization)" pargasite through pargasitic hornblende to tremolite.

[26] Phlogopite exists in two P-type samples, 33-001 and 33-012 (Table 9). These phlogopites are chemically distinct from each other.

6. Rare Earth and Trace Elements in Clinopyroxene

[27] Two F-type and five P-type clinopyroxenes along with a single gabbroic clinopyroxene were analyzed in situ for rare earth elements (REEs), Zr and Ti using two Cameca IMS-3f ion microprobes both at the Tokyo Institute of Technology and the Woods Hole Oceanographic Institution (Table 10). Analytical procedures are described in *Ohara et al.* [2002] and references therein.

[28] Chondrite-normalized REE patterns for clinopyroxenes are shown in Figure 8. Two F-type clinopyroxenes exhibit moderately sloping light to middle REE (LREE-MREE) depleted patterns, similar to those from Vulcan FZ peridotites [*Johnson et al.*, 1990]. The weak negative Eu anomaly in a single F-type clinopyroxene (D2-018) may result from analytical uncertainty. P-type clinopyroxenes, on the other hand, show relatively flat REE patterns with slightly plunging LREE and flat to humped MREE to heavy REE (HREE), quite distinct from the F-type clinopyroxenes. The P-type clinopyroxenes exhibit negative Eu anomalies, suggesting that the equilibrium melt experienced plagioclase fractionation. The gabbroic clinopyroxene (33-207) exhibits a flat, enriched REE pattern with a negative Eu anomaly, also suggesting that the equilibrium melt experienced plagioclase fractionation.

7. Discussion

7.1. Petrological Characteristics of Parece Vela Rift Peridotite

[29] The slightly deformed porphyroclastic textures, the mineral modes, the refractory mineral compositions of PVR peridotites all indicate an origin as residues of mantle melting. Parece Vela Rift peridotites have the following distinct characteristics: (1) Near least-depleted peridotite (F-type) exists. (2) Dunite (D-type) is a major lithology. (3) Plagioclase-bearing peridotite (P-type) is also a major lithology. The first characteristic suggests that the upper mantle beneath the relatively fast-spread PVR primarily consists of near least-depleted peridotite. This is anomalous, because the degree of mantle melting generally appears to correlate with spreading rate, with smaller degrees of mantle melting at slow-spreading ridge and higher degrees of mantle melting at fast-spreading ridge [e.g., *Niu and Hekinian*, 1997]. The second and third characteristics are also unique among the global abyssal peridotite suite. According to the compilation of abyssal peridotites from slow-spreading ridges [*Dick*, 1989], dunites consist of only ~0.3% (by weight) of the compiled sample suite, whereas plagioclase-bearing peridotites consist of ~20% (by number). The last two characteristics in fact suggest that melt-

Table 10. Ion Probe Analyses of Clinopyroxene in the Parece Vela Rift Peridotites and a Gabbro

	Godzilla Mullion					S3 Segment Midpoint			
	P-Type				Gabbro	F-Type		P-Type	
Sample	33-001	33-008	33-009	33-012	33-207	D2-017	D2-018	D2-005	Chondrite
No. Anal.	2	1	2	3	2	2	2	2	
					Given in ppm				
Ce	1.24 (0.01)	2.48	4.63 (0.15)	3.34 (1.52)	13.07 (3.68)	0.12 (0.01)	0.13 (0.02)	2.39 (0.06)	0.616
Pr	0.53 (0.06)	0.87	1.18 (0.04)	0.82 (0.20)	–	0.09 (0.01)	0.09 (0.01)	0.54 (0.02)	0.093
Nd	3.91 (0.26)	6.38	7.31 (0.17)	5.50 (0.64)	12.81 (0.25)	1.01 (0.07)	0.86 (0.11)	3.02 (0.00)	0.457
Sm	2.20 (0.11)	2.84	3.24 (0.17)	2.79 (0.21)	5.59 (0.08)	0.93 (0.04)	0.81 (0.02)	1.68 (0.04)	0.149
Eu	0.62 (0.02)	0.65	0.89 (0.01)	0.94 (0.14)	1.67 (0.10)	0.39 (0.05)	0.29 (0.06)	0.50 (0.03)	0.056
Gd	2.40 (0.01)	2.78	3.56 (0.26)	2.99 (0.13)	–	1.33 (0.02)	1.26 (0.05)	2.16 (0.06)	0.197
Tb	0.48 (0.01)	0.47	0.68 (0.04)	0.61 (0.06)	–	0.31 (0.04)	0.29 (0.00)	0.46 (0.01)	0.035
Dy	3.82 (0.09)	3.34	4.64 (0.63)	4.61 (0.12)	7.61 (0.73)	2.83 (0.20)	2.69 (0.19)	3.53 (0.02)	0.245
Ho	0.70 (0.06)	0.62	0.85 (0.19)	0.88 (0.06)	–	0.61 (0.04)	0.54 (0.00)	0.71 (0.01)	0.055
Er	2.06 (0.15)	1.70	2.77 (0.58)	2.54 (0.16)	4.05 (0.66)	1.86 (0.04)	1.67 (0.10)	2.27 (0.06)	0.160
Tm	0.30 (0.05)	0.25	0.36 (0.04)	0.36 (0.03)	–	0.29 (0.03)	0.26 (0.01)	0.30 (0.01)	0.025
Yb	1.79 (0.16)	1.53	2.28 (0.34)	2.05 (0.19)	4.03 (0.56)	1.68 (0.20)	1.55 (0.03)	1.86 (0.03)	0.159
Lu	0.32 (0.02)	0.23	0.38 (0.09)	0.33 (0.03)	–	0.26 (0.01)	0.24 (0.02)	0.30 (0.01)	0.024
No. Anal.	1	1	1	1	–	1	1	1	
Ti	1997	1348	1545	2056	–	1420	1390	2432	436
Zr	8.5	16.0	17.9	14.0	–	2.0	1.8	11.7	3.9
Laboratory	TITECH	TITECH	TITECH	TITECH	WHOI	TITECH	TITECH	TITECH	

No. Anal., Number of analyses making up the average composition. Numbers in parentheses are standard deviations (1 sigma). TITECH, Tokyo Institute of Technology; WHOI, Woods Hole Oceanographic Institution. Chondrite composition from *Anders and Ebihara* [1982].

mantle interaction was important in the upper mantle beneath the PVR (see discussions below).

[30] The Romanche FZ yields plagioclase-bearing peridotites with subordinate undepleted peridotites (spinel Cr # ~0.10) [*Bonatti et al.*, 1992, 1993; *Seyler and Bonatti*, 1997], similar to the situation in the PVR. *Bonatti et al.* [1992, 1993] suggested that the upper mantle beneath the equatorial MAR has undergone little or no melting due to the presence of cold upper mantle, and inferred that undepleted peridotite is left unaffected at some part of the Romanche FZ by the process which generated plagioclase-bearing peridotite. In the following discussion, we will compare Romanche peridotite with PVR peridotite in order to better characterize the petrogenesis of PVR peridotite.

7.2. Small Degree of Mantle Melting at the Relatively Fast-Spread Parece Vela Rift

[31] The tectonic characteristics noted in section 2, peridotite exposure at a segment midpoint, and the existence of near least-depleted peridotites all indicate a small degree of mantle melting beneath the

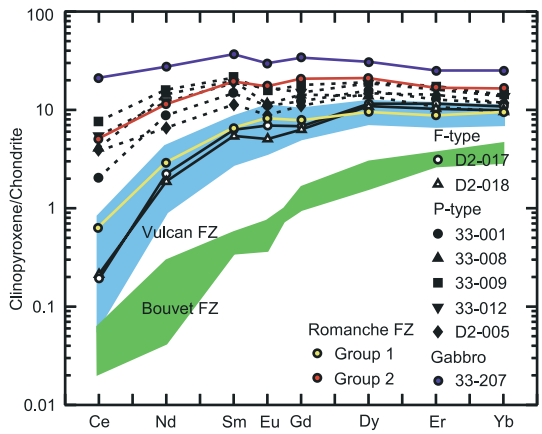

Figure 8. Chondrite-normalized REE patterns of clinopyroxenes from Parece Vela Rift peridotites and gabbro. Data for clinopyroxenes from the Vulcan and Bouvet FZ are shown for comparison [*Johnson et al.*, 1990]. Chondrite normalizing values are from *Anders and Ebihara* [1982]. The Gd value for the gabbroic sample 33-207 is interpolated. Note the relatively flat REE patterns with Eu anomaly for P-types. Mean compositions of clinopyroxenes from Romanche FZ Group 1 and Group 2 (plagioclase-bearing) peridotites [data from *Seyler and Bonatti*, 1997] are plotted for comparison. The Vulcan and Bouvet FZ data define the upper and lower limits of REE concentrations in the clinopyroxenes studied by *Johnson et al.* [1990], respectively.

PVR, despite the basin's relatively fast-spreading rates. Ohara et al. (submitted manuscript, 2003) suggest these anomalous characteristics result from an extreme transform fault effect caused by the ridge-transform geometry of short first-order segments sandwiched by closely spaced fracture zones. Ohara et al. (submitted manuscript, 2003) thus propose a hypothesis, the ''transform sandwich effect'', which significantly inhibited mantle melting beneath the relatively fast-spread PVR.

7.3. Origin of F-Type

[32] The most fertile peridotites from the Romanche FZ have average modal compositions (Table 3 [*Seyler and Bonatti*, 1997]) very close to pyrolite (olivine, 60%; orthopyroxene, 25%; clinopyroxene, 15% [*Bonatti et al.*, 1993]). In contrast, the proportion of clinopyroxene in F-type is exceptionally low (Table 3; Figure 3), despite its near least-depleted mineral composition; we may have underestimated modal clinopyroxene due to extensive serpentinization. The high proportion of modal orthopyroxene for F-type may reflect the fact that some clinopyroxene grains were counted as orthopyroxene. The original lithology thus should be lherzolite, not harzburgite.

[33] Although F-types are slightly more depleted than Romanche Group 1 peridotites, we interpret that F-types are still ''near least-depleted'' in a global sense with mineral compositions that consistently plot in the near least-depleted end of the abyssal peridotite range (Figures 5–8). Melting models developed by *Johnson et al.* [1990] and *Sobolev and Shimizu* [1992] indicate that F-type experienced ~4% near-fractional melting of a depleted MORB-type mantle (see *Ohara et al.* [2002] for modeling parameters). We thus propose that F-type peridotites are derived from an ''intact'' fragment of the residue of earlier melting event beneath the PVR, which was left unaffected by the process which created D- and P-types (see 7-4 and 7-5). *Seyler and Bonatti* [1997] found Al-rich spinel and clinopyroxene inclusions within Al-poor orthopyroxene grains in a single Romanche plagioclase-bearing peridotite. They thus inferred that these Al-rich phases are relics of an earlier, more fertile mineral assemblage.

[34] F-types may alternatively be the residues of larger degrees of mantle melting which were later refertilized by reaction with migrating melt [*Elthon*, 1992]. However, negligible amount of TiO_2 in F-type spinels suggests this possibility is unlikely, because it is generally accepted that Ti and Cr contents in spinel increase due to melt-rock interaction [*Dick and Bullen*, 1984]. The tectonic characteristics noted in section 2 along with peridotite exposure at a segment midpoint indicate a small degree of mantle melting beneath the PVR, also ruling out the refertilized origin of F-type.

7.4. Origin of D-Type

[35] Dunites within mantle section of ophiolites have been interpreted as residues of very high degrees of melting (~40% melting), olivine cumulate dikes, or replacive dunites [*Kelemen et al.*, 1995, 1997, and references therein].

[36] In agreement with the reasoning by *Kelemen et al.* [1995, 1997], we interpret that D-types are replacive dunites formed by reaction of olivine-saturated melt from a relatively high-pressure with pyroxene-bearing wall rock peridotite (i.e., F-type) at a lower pressure at high melt/rock ratio, dissolving pyroxene and precipitating olivine within and around conduits for focused melt (basalt) extraction in mantle (reaction melt 1 + pyroxene = melt 2 + olivine + spinel). D-type spinel is almost constant in composition with Cr # ~0.42 and Mg # ~0.65 (Figure 5a), similar to the spinel (Cr # ~0.43 and Mg # ~0.68) in the spatially associated tholeiitic basalts drilled at Site 449 during DSDP Leg 59 (the location is shown in Figure 2 [*Mattey et al.*, 1980]). The spinel compositions suggest that D-type and the spatially associated basalt are in equilibrium.

[37] Although extensive formation of dunite is most likely in upwelling asthenospheric mantle, replacive dunites can also form in shallow lithospheric mantle in ductile shear zones or in porous reaction zones around propagating cracks [*Kelemen et al.*, 1995, 1997, and references therein]. Since we lack the direct field evidence for the PVR sample suite, we cannot tell at this time whether D-type samples are products of an asthenospheric process or a lithospheric process.

7.5. Origin of P-Type

[38] The presence of plagioclase in peridotite has been explained by the following mechanisms: (1) Reequilibration of an ascending mantle body as it moves from spinel- to plagioclase-peridotite facies field through reaction orthopyroxene + clinopyroxene + Al-spinel = olivine + plagioclase + Cr-spinel [*Frost*, 1976; *Hamlyn and Bonatti*, 1980]. (2) Impregnation of residual peridotite by either in situ or exotic melt through reaction melt + Al-spinel = plagioclase + Cr-spinel [*Church and Stevens*, 1971; *Dick and Bullen*, 1984; *Dick and Fisher*, 1984; *Dick*, 1989].

[39] Both mechanisms can account for Cr-enrichment in spinel in plagioclase-bearing peridotite. However, the occurrence of fertile F-type with depleted D- and P-types in the same dredge haul (KR98-1-D2) rules out the former mechanism, because no fragments of spinel-peridotite could have been preserved at a single-dredge-haul scale. We alternatively interpret that P-type was formed through the latter mechanism, where residual peridotite (i.e., F-type) reacted with melt migrating by diffuse porous flow at low melt/rock ratio, possibly in conductively cooled shallow lithospheric mantle. The distinct composition of P-type (i.e., the degree of depletion estimated from spinel and pyroxene compositions is higher than F-type, while these minerals are enriched in incompatible elements; Figures 5–8) is consistent with the latter mechanism. Coexistence of D- and P-types in the same dredge haul may further suggest that the reacted melt was possibly derived from the parental melt that involved in D-type formation.

7.6. Origin of Gabbro

[40] Dredge CSS33-D1 recovered gabbros along with P-type peridotites. The fractionated major element compositions of gabbroic pyroxenes (Figures 6 and 7) and enriched REE concentration in the clinopyroxene (Figure 8) clearly indicate that PVR gabbros are not in chemical equilibrium with P-type (nor F- and D-types). We infer that these evolved gabbros formed in equilibrium with evolved melts more enriched in incompatible elements than the spatially associated tholeiitic basalts, by combination of melt-mantle interaction and extensive crystal fractionation within a conductively cooled lithosphere [*Kelemen et al.*, 1997]. These evolved gabbros therefore may represent shallow level cumulates formed in small and transient magma chambers expected at ridge-transform intersections of slow-spreading ridges. Intrusive relationships between evolved gabbro and mantle peridotite are characteristic of magma-starved ridge environments [*Cannat et al.*, 1992]. Parece Vela Rift gabbros contain deformed plagioclase grains (Figure 4g), indicating syn-tectonic intrusion. We thus interpret that PVR gabbros are evolved dikes or sills intruded into P-type peridotite at the apparently magma-starved PVR.

7.7. Origin of Hydrous Minerals in Peridotites

[41] "Primary" hydrous minerals exist in F- and P-type peridotites. The Ti- and K-rich chemistry of some amphiboles in PVR peridotites (Table 8) is similar to that of the pargasite from Zabargad Island peridotites, which represent undepleted, metasomatized parental mantle of the Red Sea lithosphere [*Bonatti et al.*, 1986]. However, the observation that phlogopite is not ubiquitous (only two samples) and these two phlogopites have distinct major element compositions (Ti, Na and K contents; Table 9), may suggest an alternative interpretation that these hydrous minerals are formed by seawater circulation. There is no evidence of melt-mantle interaction (or metasomatism by fluid) in the least-depleted F-type sample (D2-017), yet it includes pargasite. This observation also suggests that pargasite in F-type is a late product of relatively high temperature seawater circulation (possibly prior to serpentinization), not related to primary melt-mantle interaction, or to an originally metasomatized mantle domain.

8. Summary

[42] As a summary, we propose the following lithospheric processes beneath the PVR:

[43] 1. Owing to a "transform sandwich effect (Ohara et al., submitted manuscript, 2003)", the short first-order segments experienced a small

degree of near-fractional melting of a depleted MORB-type mantle beneath the PVR, leaving a near least-depleted residue (F-type) among the global abyssal peridotite suite.

[44] 2. Melt from a relatively high pressure reacted with F-type at a lower pressure at high melt/rock ratio and created D-type.

[45] 3. Some melt migrating by diffuse porous flow further reacted with F-type at low melt/rock ratio possibly in conductively cooled shallow lithospheric mantle, forming P-type.

[46] 4. Shallow level fractionated melt intruded into P-type peridotite, forming dikes or sills of evolved gabbro.

[47] 5. High temperature seawater circulation precipitated ''primary'' amphibole and phlogopite (i.e., before serpentinization) in F- and P-type peridotites.

Acknowledgments

[48] We are grateful to the captains, crews and scientists aboard S/V Takuyo and R/V Kairei for their support. Parts of this study were done at the Woods Hole Oceanographic Institution during Y.O.'s stay at Henry Dick's laboratory in 2001. Y.O. thank Henry Dick for discussion and encouragement and Nobumichi Shimizu for his help on the ion microprobe at Woods Hole. We thank Kazuhito Ozawa, Kensaku Tamaki, Jonathan Snow and Kyoko Okino for discussions. We are indebted to Tsuyoshi Yoshida for bathymetric data processing. Comments from Robert Stern improved the initial manuscript. Constructive reviews from William White (as editor), Peter Kelemen (as guest editor), Shoji Arai and two anonymous referees were helpful to revise the manuscript. GMT 3.0 [*Wessel and Smith*, 1995] was used to map bathymetric data.

References

Anders, E., and M. Ebihara, Solar-system abundances of the elements, *Geochim. Cosmochim. Acta*, *46*, 2363–2380, 1982.

Aumento, F., and H. Loubat, The Mid-Atlantic Ridge near 45°N, XVI: Serpentinized ultramafic intrusions, *Can. J. Earth Sci.*, *8*, 631–663, 1970.

Bence, A. E., and A. L. Albee, Empirical correction factors for the electron microanalysis of silicates and oxides, *J. Geol.*, *76*, 382–403, 1968.

Blackman, D., J. R. Cann, B. Janssen, and D. Smith, Origin of extensional core complexes: Evidence from the Mid-Atlantic Ridge at Atlantis Fracture Zone, *J. Geophys. Res.*, *103*, 21,315–21,333, 1998.

Bloomer, S. H., B. Taylor, C. J. MacLeod, R. J. Stern, P. Fryer, J. Hawkins, and L. Johnson, Early arc volcanism and ophiolite problem: A perspective from drilling in the Western Pacific, in *Active Margins and Marginal Basins of the Western Pacific*, *Geophys. Monogr. Ser.*, vol. 88, edited by B. Taylor and J. Natland, pp. 1–30, AGU, Washington, D. C., 1995.

Bogdanov, N., (Ed.), Initial report of the geological study of the oceanic crust of the Philippine Sea floor: Investigations by the international working group on the IGCP project ''Ophiolites'' (R/V Dmitry Mendeleev cruise 17, June–August 1976), *Ofioliti*, *2*, 137–168, 1977.

Bonatti, E., G. Ottonello, and P. R. Hamlyn, Peridotites from the island of Zabargad (St. John), Red Sea: Petrology and geochemistry, *J. Geophys. Res.*, *91*, 599–631, 1986.

Bonatti, E., A. Peyve, P. Kepezhinskas, N. Kurentsova, M. Seyler, S. Skolotnev, and G. Udintsev, Upper mantle heterogeneity below the Mid-Atlantic Ridge, 0°–15°N, *J. Geophys. Res.*, *97*, 4461–4476, 1992.

Bonatti, E., M. Seyler, and N. Sushevskaya, A cold suboceanic mantle belt at the Earth's equator, *Science*, *261*, 315–320, 1993.

Cann, J. R., D. K. Blackman, D. K. Smith, E. McAllister, B. Janssen, S. Mello, E. Avgerinos, A. R. Pascoe, and J. Escartín, Corrugated slip surfaces formed at ridge-transform intersections on the Mid-Atlantic Ridge, *Nature*, *385*, 329–332, 1997.

Cannat, M., Emplacement of mantle rocks in the seafloor at mid-ocean ridges, *J. Geophys. Res.*, *98*, 4163–4172, 1993.

Cannat, M., D. Bideau, and H. Bougault, Serpentinized peridotites and gabbros in the Mid-Atlantic Ridge axial valley at 15°37′N and 16°52′N, *Earth Planet. Sci. Lett.*, *109*, 87–106, 1992.

Cannat, M., C. Mével, M. Maia, C. Deplus, C. Durand, P. Gente, P. Agrinier, A. Belarouchi, G. Dubuisson, E. Humler, and J. Reynolds, Thin crust, ultramafic exposures, and rugged faulting patterns at the Mid-Atlantic Ridge (22°–24°N), *Geology*, *23*, 49–52, 1995.

Church, R. W., and R. K. Stevens, Early Paleozoic ophiolite complexes of the Newfoundland Appalachians as mantle-oceanic crust sequences, *J. Geophys. Res.*, *76*, 1460–1466, 1971.

Dick, H. J. B., Abyssal peridotites, very slow spreading ridges and ocean ridge magmatism, in *Magmatism in the Ocean Basins*, edited by A. D. Saunders and M. J. Norry, *Geol. Soc. Spec. Publ.*, *42*, 71–105, 1989.

Dick, H. J. B., and T. Bullen, Chromian spinel as a petrogenetic indicator in abyssal and alpine-type peridotites and spatially associated lavas, *Contrib. Mineral. Petrol.*, *86*, 54–76, 1984.

Dick, H. J. B., and R. L. Fisher, Mineralogic studies of the residues of mantle melting: Abyssal and alpine-type peridotites, in *Kimberlites, the Mantle and Crust-Mantle Relationships*, edited by J. Kornprobst, pp. 295–308, Elsevier Sci., New York, 1984.

Dick, H. J. B., R. L. Fisher, and W. B. Bryan, Mineralogic variability of the uppermost mantle along mid-ocean ridges, *Earth Planet. Sci. Lett.*, *69*, 88–106, 1984.

Dietrich, V., R. Emmermann, R. Oberhansli, and H. Puchelt, Geochemistry of basaltic and gabbroic rocks from the west Mariana Trench, *Earth Planet. Sci. Lett.*, *39*, 127–144, 1978.

Elthon, D., Chemical trends in abyssal peridotites: Refertilization of depleted suboceanic mantle, *J. Geophys. Res.*, *97*, 9015–9025, 1992.

Frost, B. R., Limits to the assemblage forsterite-anorthite as inferred from peridotite hornfelses, Icicle Creek, Washington, *Am. Mineral.*, *61*, 732–750, 1976.

Hamlyn, P. R., and E. Bonatti, Petrology of mantle-derived ultramafics from the Owen fracture zone, northwest Indian Ocean: Implications for the nature of the oceanic upper mantle, *Earth Planet. Sci. Lett.*, *48*, 65–79, 1980.

Johnson, K. T. M., H. J. B. Dick, and N. Shimizu, Melting in the oceanic upper mantle: An ion microprobe study of diopsides in abyssal peridotites, *J. Geophys. Res.*, *95*, 2661–2678, 1990.

Kasuga, S., and Y. Ohara, A new model of back-arc spreading in the Parece Vela Basin, northwest Pacific margin, *The Island Arc*, *6*, 316–326, 1997.

Kelemen, P. B., N. Shimizu, and V. J. M. Salters, Extraction of mid-ocean-ridge basalt from the upwelling mantle by focused flow of melt in dunite channels, *Nature*, *375*, 747–753, 1995.

Kelemen, P. B., G. Hirth, N. Shimizu, M. Spiegelman, and H. J. B. Dick, A review of melt migration processes in the adiabatically upwelling mantle beneath oceanic spreading ridges, *Philos. Trans. R. Soc. London Ser. A*, *355*, 283–318, 1997.

MacLeod, C. J., et al., Direct geological evidence for oceanic detachment faulting: The Mid-Atlantic Ridge, 15°45′N, *Geology*, *30*, 879–882, 2002.

Mattey, D. P., N. G. Marsh, and J. Tarney, The geochemistry, mineralogy, and petrology of basalts from the West Philippine and Parece Vela basins and from the Palau-Kyushu and West Mariana ridges, *Deep Sea Drill. Project Inital Rep.*, *59*, 753–800, Washington, D. C., 1980.

Michael, P. J., and E. Bonatti, Peridotite composition from the North Atlantic: Regional and tectonic variations and implications for partial melting, *Earth Planet. Sci. Lett.*, *73*, 91–104, 1984.

Mitchell, N., J. Escartín, and S. Allerton, Detachment faults at mid-ocean ridges garner interest, *Eos Trans. AGU*, *79*, 127, 1998.

Miyashiro, A., F. Shido, and M. Ewing, Composition and origin of serpentinites from the Mid-Atlantic Ridge near 24° and 30° north latitude, *Contrib. Mineral. Petrol.*, *23*, 117–127, 1969.

Niu, Y., and R. Hekinian, Spreading-rate dependence of the extent of mantle melting beneath ocean ridges, *Nature*, *385*, 326–329, 1997.

Ohara, Y., S. Kasuga, and T. Ishii, Peridotites from the Parece Vela Rift in the Philippine Sea: Upper mantle material exposed in an extinct backarc basin, *Proc. Jpn. Acad. Ser. B*, *72*, 118–123, 1996.

Ohara, Y., T. Yoshida, Y. Kato, and S. Kasuga, Giant megamullion in the Parece Vela backarc basin, *Mar. Geophys. Res.*, *22*, 47–61, 2001.

Ohara, Y., R. J. Stern, T. Ishii, H. Yurimoto, and T. Yamazaki, Peridotites from the Mariana Trough: First look at the mantle beneath an active backarc basin, *Contrib. Mineral. Petrol.*, *143*, 1–18, 2002.

Ohara, Y., K. Okino, and J. E. Snow, KR03-01 shipboard scientific party, Preliminary report of Kairei KR03-01 cruise: Amagmatic tectonics and lithospheric composition of the Parece Vela Basin, *InterRidge News*, *12*, 27–29, 2003.

Okino, K., S. Kasuga, and Y. Ohara, A new scenario of the Parece Vela Basin genesis, *Mar. Geophys. Res.*, *20*, 21–40, 1998.

Okino, K., Y. Ohara, S. Kasuga, and Y. Kato, The Philippine Sea: New survey results reveal the structure and the history of the marginal basins, *Geophys. Res. Lett.*, *26*, 2287–2290, 1999.

Park, C., K. Tamaki, and K. Kobayashi, Age-depth correlation of the Philippine Sea back-arc basins and other marginal basins in the world, *Tectonophysics*, *181*, 351–371, 1990.

Sandwell, D. T., and W. H. F. Smith, Marine gravity anomaly from Geosat and ERS 1 satellite altimetry, *J. Geophys. Res.*, *102*, 10,039–10,054, 1997.

Seyler, M., and E. Bonatti, Regional-scale melt-rock interaction in lherzolitic mantle in the Romanche Fracture Zone (Atlantic Ocean), *Earth Planet. Sci. Lett.*, *146*, 273–287, 1997.

Shcheka, S. A., S. V. Vysotskiy, V. T. S'edin, and I. A. Tararin, Igneous rocks of the main geological structures of the Philippine Sea floor, in *Geology and Geophysics of the Philippine Sea*, edited by H. Tokuyama et al., pp. 251–278, Terra Sci., Tokyo, 1995.

Sobolev, A. V., and N. Shimizu, Superdepleted melts and ocean mantle permeability, *Dokl. Rossiyskoy Akademii Nauk*, *326*, 354–360, 1992.

Stern, R. J., S. H. Bloomer, F. Martinez, T. Yamazaki, and T. M. Harrison, The composition of backarc basin lower crust and upper mantle in the Mariana Trough: A first report, *The Island Arc*, *5*, 354–372, 1996.

Stern, R. J., T. Yamazaki, S. Danishwar, and C.-H. Sun, Back-arc basin lower crust and upper mantle in the northern Mariana Trough studied with "Shinkai 6500", *J. Deep Sea Res.*, *13*, 47–61, 1997.

Tucholke, B., and J. Lin, A geological model for the structure of ridge segments in slow spreading ocean crust, *J. Geophys. Res.*, *99*, 11,937–11,958, 1994.

Tucholke, B., J. Lin, and M. Kleinrock, Megamullions and mullion structure defining oceanic metamorphic core complexes on the Mid-Atlantic Ridge, *J. Geophys. Res.*, *103*, 9857–9866, 1998.

Wessel, P., and W. H. F. Smith, New version of the Generic Mapping Tools released, *Eos Trans. AGU*, *76*, 329, 1995.